Astrodynamics Vol. 4, No. 1, 1–16, 2020 https://doi.org/10.1007/s42064-019-0068-7

Non-equatorial equilibrium points around an asteroid with gravitational orbit–attitude coupling perturbation

Yue Wang (✉), **Shijie Xu**

School of Astronautics, Beihang University, Beijing 102206, China

ABSTRACT

A recently proposed orbital dynamics model in the close proximity of an asteroid, which is called "attitude-restricted orbital dynamics", includes the perturbation caused by the spacecraft's gravitational orbit–attitude coupling. This orbital model improves the precision of classical point-mass orbital model with only the non-spherical gravity. Equatorial equilibrium points have been investigated in the previous paper. In this paper, the in-plane non-equatorial equilibrium points, which are outside the asteroid's equatorial plane but within its longitudinal principal plane, are further studied for a uniformly-rotating asteroid. These non-equatorial equilibrium points are more diverse than those in the classical point-mass orbital dynamics without gravitational orbit–attitude coupling perturbation (GOACP). Two families of them have been found. The equatorial equilibrium points studied before and the non-equatorial ones studied here give a complete map of equilibrium points in the asteroid's principal planes. Compared with the classical point-mass orbital dynamics without GOACP, the equatorial equilibrium points have extended the longitude range of equilibrium points around an asteroid, while the non-equatorial ones studied here will extend the latitude range. These equatorial and non-equatorial equilibrium points provide natural hovering positions for the asteroid close-proximity operations.

KEYWORDS

asteroid mission

gravitational orbit–attitude coupling perturbation (GOACP)

attitude-restricted orbital dynamics

non-equatorial equilibrium points

Research Article

Received: 20 November 2018

Accepted: 9 August 2019

1 Introduction

Driven by great interests of the space community in asteroid missions, spacecraft dynamics about asteroids has been an active research area in recent years. In the close proximity of a small asteroid, due to the large ratio of the spacecraft's dimension to the orbit radius, significant gravitational coupling may exist between the orbital and attitude motions of a large-sized spacecraft. This issue was first raised by Scheeres [1] and was assessed by Wang and Xu through numerical simulations [2]. The precision of the traditional modeling approach, in which the spacecraft is treated as a point mass in orbital dynamics [3–8], and the attitude motion is studied restrictedly on a predetermined orbit [9–12], can be improved by including the gravitational orbit–attitude coupling.

The gravitationally coupled orbit–attitude dynamics (also called "full dynamics" in some previous papers), in which the spacecraft is modeled as an extended rigid body, has been proposed to include the gravitational orbit–attitude coupling. Qualitative properties of gravitationally coupled orbit–attitude dynamics (full dynamics) of a rigid spacecraft, including the relative equilibria and stability, have been studied in a spherical gravity field [13–17], in the gravity field of a spheroid asteroid truncated on the second zonal harmonic J_2 [18], and in the gravity field of an asteroid truncated on the second degree and order harmonics C_{20} and C_{22} [19]. Besides, the gravitationally coupled orbit–attitude dynamics has been used in the studies of navigation and control of the close-proximity operations [20–22].

From the perspective of orbital dynamics, the gravitational orbit–attitude coupling causes another orbital perturbation besides the asteroid's non-spherical gravity, solar radiation pressure (SRP), and solar tide. It has been shown that the ratio of gravitational orbit–attitude coupling perturbation (GOACP) to the non-

✉ ywang@buaa.edu.cn

spherical gravity of the asteroid is the order of $(\rho/a_e)^2$, where ρ is the spacecraft's characteristic dimension and a_e is the asteroid's mean radius [23]. Thus, GOACP needs to be considered for a large-sized spacecraft.

Due to this reason, the attitude-restricted orbital dynamics has been proposed to include GOACP in close-proximity orbital dynamics [24]. In this model, the spacecraft is assumed to be kept at a given attitude with respect to the asteroid, and the orbital motion perturbed by both the asteroid's non-spherical gravity and GOACP is studied. The word "restricted" means that the orbital motion is studied as a restricted problem at a given attitude. As stated by Wang and Xu [24], the traditional spacecraft dynamics and the attitude-restricted orbital dynamics are two different approximations of the exact motion. Wang and Xu have shown that GOACP makes the phase space of the system quite different from the classical point-mass orbital dynamics without GOACP [24]. In that paper, two kinds of equatorial equilibrium points were obtained: on and off the asteroid's equatorial principal axes, which extends the longitude range of classical equilibrium points without GOACP.

In this paper, we used the same dynamical model as in Wang and Xu [24], to further investigate the in-plane non-equatorial equilibrium points about a uniformly-rotating asteroid. These non-equatorial equilibrium points will extend the latitude range of classical equilibrium points without GOACP, and will provide more natural hovering positions for the close-proximity operations. The paper is organized as follows: the equations of motion and equilibrium conditions are given in Section 2 and Section 3, respectively, followed by iteration methods for solving equilibrium points in Section 4. Then, in-plane non-equatorial equilibrium points are calculated and analyzed in details in Section 5. Finally, the paper is concluded in Section 6.

2 System description and equations of motion

The system studied here is the same as that in Wang and Xu [24]. Here we will give a brief description about the dynamical model.

As described by Fig. 1, the orbital motion of a rigid spacecraft B moving around a small asteroid P is considered. It is assumed that the asteroid is rotating

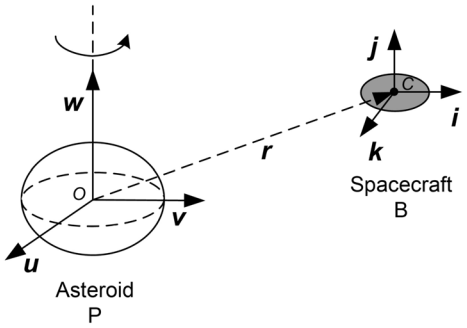

Fig. 1 Spacecraft moving around a small asteroid. Reproduced with permission from Ref. [24], © Springer Science+Bussiness Media Dordrecht 2015.

uniformly around its maximum-moment principal axis at angular velocity ω_T. The body-fixed principal-axis reference frames of the asteroid and the spacecraft are given by $S_{\rm P} = (\boldsymbol{u}, \boldsymbol{v}, \boldsymbol{w})$ and $S_{\rm B} = (\boldsymbol{i}, \boldsymbol{j}, \boldsymbol{k})$ with O and C as their origins, respectively. The origin of the frame $S_{\rm P}$ is fixed at the center of mass of the asteroid, and the coordinate axes are chosen to be aligned along the principal moments of inertia of the asteroid. Then, the asteroid's gravity field up to the second degree and order can be represented by the harmonic coefficients C_{20} and C_{22} with other harmonic coefficients vanished [25].

The attitude of spacecraft is described with respect to the asteroid by $\boldsymbol{A}$:

$$\boldsymbol{A} = [\boldsymbol{\alpha},\ \boldsymbol{\beta},\ \boldsymbol{\gamma}]^{\rm T} \in SO(3) \tag{1}$$

where vectors $\boldsymbol{\alpha}$, $\boldsymbol{\beta}$, and $\boldsymbol{\gamma}$ are coordinates of $\boldsymbol{u}$, $\boldsymbol{v}$, and $\boldsymbol{w}$ expressed in the spacecraft's frame $S_{\rm B}$, respectively. The spacecraft's position vector expressed in the asteroid's frame $S_{\rm P}$ is denoted by $\boldsymbol{r} = [x,\ y,\ z]^{\rm T}$, and $\bar{\boldsymbol{r}} = [\bar{x},\ \bar{y},\ \bar{z}]^{\rm T}$ is the unit vector along $\boldsymbol{r}$. The spacecraft's mass and inertia tensor expressed in the body-fixed frame $S_{\rm B}$ are denoted by m and $\boldsymbol{I} = {\rm diag}\{I_{xx},\ I_{yy},\ I_{zz}\}$, respectively.

Equations of orbital motion expressed in the body-fixed frame of the uniformly rotating asteroid are given by Scheeres [4]

$$\ddot{\boldsymbol{r}} + 2\boldsymbol{\omega}_T \times \dot{\boldsymbol{r}} + \boldsymbol{\omega}_T \times \boldsymbol{\omega}_T \times \boldsymbol{r} = \boldsymbol{\alpha}_{\rm s/c} \tag{2}$$

where $\boldsymbol{\alpha}_{\rm s/c}$ is the spacecraft's acceleration and $\boldsymbol{\omega}_T = [0,\ 0,\ \omega_T]^{\rm T}$.

As in Wang and Xu [24], in the attitude-restricted orbital dynamics, the perturbation of the asteroid's non-spherical gravity and GOACP are considered, and the less significant perturbations of the SRP and solar tide are neglected.

According to Wang *et al.* [23], a very large spacecraft ($\rho > 100$ m), such as a gravity tractor, actually has a lower area-to-mass ratio (AMR) than a standard-size spacecraft, because, as ρ increases, the area increases with ρ^2 but the mass increases with a ratio between ρ^2 and ρ^3. As a result, the SRP effect of a large spacecraft is weaker than that of a standard-size spacecraft. Based on the results in Wang *et al.* [23], it can be estimated that, for cases considered in this paper, a very large spacecraft ($\rho > 100$ m) with a distance of about 400 m w.r.t. a small asteroid, the GOACP can be two orders of magnitude larger than the SRP. Therefore, we will neglect the SRP effect and then an analytical investigation will be possible.

Then, the acceleration $\boldsymbol{\alpha}_{\mathrm{s/c}}$ is given by

$$\boldsymbol{\alpha}_{\mathrm{s/c}} = \boldsymbol{\alpha}_{\mathrm{Kepler}} + \boldsymbol{\alpha}_{\mathrm{NSG}} + \boldsymbol{\alpha}_{\mathrm{OAC}} \tag{3}$$

where $\boldsymbol{\alpha}_{\mathrm{Kepler}}$ is the Kepler two-body acceleration:

$$\boldsymbol{\alpha}_{\mathrm{Kepler}} = -\frac{\mu}{r^2}\bar{\boldsymbol{r}} \tag{4}$$

where $\mu = GM, M$ is the asteroid's mass, and G is the gravitational constant; the second-order approximation of the asteroid's non-spherical gravity perturbation $\boldsymbol{\alpha}_{\mathrm{NSG}}$ is given by

$$\begin{aligned}\boldsymbol{\alpha}_{\mathrm{NSG}} =& \frac{3\mu}{2r^4}\Big\{ \left[\tau_0\left(1-5\bar{z}^2\right) - 10\tau_2\left(\bar{x}^2-\bar{y}^2\right)\right]\bar{\boldsymbol{r}} \\ &+ 2\tau_0\bar{z}\boldsymbol{e}_3 + 4\tau_2\left(\bar{x}\boldsymbol{e}_1 - \bar{y}\boldsymbol{e}_2\right)\Big\}\end{aligned} \tag{5}$$

where $\tau_0 = a_e^2 C_{20}$, $\tau_2 = a_e^2 C_{22}$, a_e is the asteroid's mean equatorial radius, $\boldsymbol{e}_1 = [1,\ 0,\ 0]^{\mathrm{T}}$, $\boldsymbol{e}_2 = [0,\ 1,\ 0]^{\mathrm{T}}$, and $\boldsymbol{e}_3 = [0,\ 0,\ 1]^{\mathrm{T}}$; the spacecraft's GOACP $\boldsymbol{\alpha}_{\mathrm{OAC}}$ up to the second-order terms is given by Wang and Xu [24]:

$$\begin{aligned}\boldsymbol{\alpha}_{\mathrm{OAC}} =& \frac{3\mu}{2r^4}\Bigg\{ \left[5\bar{\boldsymbol{r}}^{\mathrm{T}}\boldsymbol{A}\left(\frac{\boldsymbol{I}}{m}\right)\boldsymbol{A}^{\mathrm{T}}\bar{\boldsymbol{r}} - \mathrm{tr}\left(\frac{\boldsymbol{I}}{m}\right)\right]\bar{\boldsymbol{r}} \\ &- 2\boldsymbol{A}\left(\frac{\boldsymbol{I}}{m}\right)\boldsymbol{A}^{\mathrm{T}}\bar{\boldsymbol{r}}\Bigg\}\end{aligned} \tag{6}$$

From the point of view of two bodies interacting through the mutual potential, the Kepler two-body acceleration $\boldsymbol{\alpha}_{\mathrm{Kepler}}$ is the zeroth-order term, or second-order term in $1/r$, while the non-spherical gravity perturbation $\boldsymbol{\alpha}_{\mathrm{NSG}}$ and the GOACP $\boldsymbol{\alpha}_{\mathrm{OAC}}$ are both second-order terms, or fourth-order terms in $1/r$. See Wang and Xu [24] for detailed discussions on the gravitational force model $\boldsymbol{\alpha}_{\mathrm{s/c}}$.

For an irregular-shaped asteroid, the higher-order terms of non-spherical gravity are also of importance in the close proximity of the asteroid. According to Wang *et al.* [23], the ratio of GOACP to the second-order non-spherical gravity of the asteroid is the order of $(\rho/a_e)^2$, where ρ is the spacecraft's characteristic dimension and a_e is the asteroid's mean radius. Therefore, for a very large spacecraft ($\rho > 100$ m) near a small asteroid with a similar size, the GOACP can have the same order of magnitude with the second-order non-spherical gravity. Among the higher-order non-spherical gravity, the third-order terms will be the most significant. Based on the results in Wang *et al.* [23], it can be found that, the ratio of the GOACP to the third-order non-spherical gravity is the order of $(\rho/a_e)^2(r/a_e)$, where r is the distance of the spacecraft w.r.t. the asteroid. Usually, we have $r/a_e > 1$, and then the GOACP will be more significant than the third-order non-spherical gravity for a very large spacecraft. Therefore, we will neglect higher-order terms of the non-spherical gravity in this study.

The perturbation $\boldsymbol{\alpha}_{\mathrm{OAC}}$ depends on the parameter $\boldsymbol{I}/m$, which actually can be described by three parameters: the mass distribution parameters σ_x and σ_y, and the characteristic dimension ρ. σ_x and σ_y are defined as

$$\sigma_x = \left(I_{zz} - I_{yy}\right)/I_{xx}, \quad \sigma_y = \left(I_{zz} - I_{xx}\right)/I_{yy} \tag{7}$$

with ranges $-1 \leqslant \sigma_x \leqslant 1$ and $-1 \leqslant \sigma_y \leqslant 1$. The characteristic dimension ρ, which is an estimation of the spacecraft's size, is defined by $\rho^2 = 2I_{xx}/m$. The GOACP $\boldsymbol{\alpha}_{\mathrm{OAC}}$ will be more significant in the case of a larger ratio of ρ to the orbital radius r or a more non-spherical mass distribution.

3 Conditions for non-equatorial equilibrium points

The equilibrium point means that the spacecraft is stationary in the asteroid's body-fixed frame, i.e., moving on a stationary orbit. Setting $\ddot{\boldsymbol{r}} = \boldsymbol{0}$ and $\dot{\boldsymbol{r}} = \boldsymbol{0}$ in the equations of motion (2), we obtain the equilibrium condition

$$\boldsymbol{\omega}_T \times \boldsymbol{\omega}_T \times \boldsymbol{r} = \boldsymbol{\alpha}_{\mathrm{s/c}} \tag{8}$$

which means that the gravitational force balances the centrifugal force of the circular orbital motion. By using Eqs. (3)–(6), the equilibrium condition in Eq. (8) can be

written as

$$\begin{aligned}\boldsymbol{\omega}_T\times\boldsymbol{\omega}_T\times\boldsymbol{r}=&-\frac{\mu}{r^2}\bar{\boldsymbol{r}}+\frac{3\mu}{2r^4}\Big\{\left[\tau_0\left(1-5\bar{z}^2\right)-10\tau_2\left(\bar{x}^2-\bar{y}^2\right)\right]\bar{\boldsymbol{r}}\\&+2\tau_0\bar{z}\boldsymbol{e}_3+4\tau_2\left(\bar{x}\boldsymbol{e}_1-\bar{y}\boldsymbol{e}_2\right)\Big\}\\&+\frac{3\mu}{2r^4}\left\{\left[5\bar{\boldsymbol{r}}^{\mathrm{T}}\boldsymbol{A}\left(\frac{\boldsymbol{I}}{m}\right)\boldsymbol{A}^{\mathrm{T}}\bar{\boldsymbol{r}}-\mathrm{tr}\left(\frac{\boldsymbol{I}}{m}\right)\right]\bar{\boldsymbol{r}}\right.\\&\left.-2\boldsymbol{A}\left(\frac{\boldsymbol{I}}{m}\right)\boldsymbol{A}^{\mathrm{T}}\bar{\boldsymbol{r}}\right\}\end{aligned}\tag{9}$$

As for the stability of equilibrium points, we have given the stability conditions in the previous paper [24]. It is found that the linear stability requires all eigenvalues of the linearized system matrix at the equilibrium point to be purely imaginary. Since the gradient of the gravitational acceleration is tedious, it is hard to obtain the characteristic polynomial of the linearized system matrix. Besides, the stability depends on parameters of both the asteroid and the spacecraft. Therefore, it will need a lot of work to investigate the stability thoroughly with respect to all the system parameters. In this paper, we will only focus on locations of equilibrium points, and the detailed study of stability will be given in the future.

3.1 Equilibrium points without GOACP

Howard [26] has studied both the equatorial and non-equatorial equilibrium points of classical point-mass orbital dynamics in the close proximity of an asteroid, the non-spherical gravity of which is described by harmonic coefficients C_{20} and C_{22}. In his study, only the perturbation of asteroid's non-spherical gravity was considered, i.e., the spacecraft's acceleration is given by $\boldsymbol{\alpha}_{\mathrm{s/c}}=\boldsymbol{\alpha}_{\mathrm{Kepler}}+\boldsymbol{\alpha}_{\mathrm{NSG}}$. Then, the equilibrium condition is given by

$$\begin{aligned}\boldsymbol{\omega}_T\times\boldsymbol{\omega}_T\times\boldsymbol{r}=&-\frac{\mu}{r^2}\bar{\boldsymbol{r}}+\frac{3\mu}{2r^4}\Big\{\Big[\tau_0\left(1-5\bar{z}^2\right)\\&-10\tau_2\left(\bar{x}^2-\bar{y}^2\right)\Big]\bar{\boldsymbol{r}}\\&+2\tau_0\bar{z}\boldsymbol{e}_3+4\tau_2\left(\bar{x}\boldsymbol{e}_1-\bar{y}\boldsymbol{e}_2\right)\Big\}\end{aligned}\tag{10}$$

Based on the equilibrium condition in Eq. (10), Howard [26] has determined both the equatorial and non-equatorial equilibrium points of the system. Consistent with the results by Hu [25], the equatorial equilibrium points are located at four longitudes: $0, \pi/2$, π, and $3\pi/2$, which can be divided into two groups, and lie on the $\boldsymbol{u}$-axis and lie on the $\boldsymbol{v}$-axis, respectively.

However, the existence of non-equatorial equilibrium points is quite limited: the non-equatorial equilibrium points can only exist within the asteroid's principal plane spanned by $\boldsymbol{w}$-axis and the shorter equatorial principal axis when some other conditions are satisfied. That is to say, non-equatorial equilibrium points, if exist, are located within the $\boldsymbol{u}$–$\boldsymbol{w}$ plane in the case of a negative C_{22} or within the $\boldsymbol{v}$–$\boldsymbol{w}$ plane in the case of a positive C_{22}. Besides, non-equatorial equilibrium points, if exist, will appear as a quadruplet, which have the same orbital radius and the same absolute value of latitude. The latitude of non-equatorial equilibrium points is determined by the asteroid's parameters μ, ω_T, τ_0, and τ_2. Therefore, in the classical point-mass orbital dynamics without GOACP, non-equatorial equilibrium points, if exist, can only exist at two longitudes $(0, \pi)$ or $(\pi/2,\ 3\pi/2)$, depending on the sign of the ellipticity C_{22}, and can only exist at one absolute value of latitude, which is determined by the asteroid's parameters. It is impossible to have non-equatorial equilibrium points at other longitudes or latitudes.

3.2 Equilibrium points with GOACP

As shown by Eq. (9), the GOACP introduces several new parameters into the system, including the attitude $\boldsymbol{A}$ and parameter $\boldsymbol{I}/m$. Therefore, the system is more complicated than the classical system in Eq. (10), and the equilibrium points will be more diverse.

After the work by Wang and Xu [24], we want to further study the non-equatorial equilibrium points. In the present paper, we will focus on the in-plane non-equatorial equilibrium points, which are located in the asteroid's longitudinal principal plane, i.e., the $\boldsymbol{u}$–$\boldsymbol{w}$ plane or $\boldsymbol{v}$–$\boldsymbol{w}$ plane. These non-equatorial equilibrium points will extend the latitude range of equilibrium points compared with the classical orbital dynamics without GOACP, and provide more potential for asteroid close-proximity operations, such as the asteroid body-fixed hovering.

Without loss of generality, we assume that the non-equatorial equilibrium point is located within the $\boldsymbol{u}$–$\boldsymbol{w}$ plane. The case within the $\boldsymbol{v}$–$\boldsymbol{w}$ plane can be converted into this case easily by changing the arrangement of $\boldsymbol{u}$ and $\boldsymbol{v}$ axes of the asteroid's body-fixed frame S_{P}. If the spacecraft is located within the $\boldsymbol{u}$–$\boldsymbol{w}$ plane, we have $\bar{x}\neq 0, \bar{y}=0, \bar{z}\neq 0$, and $\bar{\boldsymbol{r}}=[\bar{x},\ 0,\ \bar{z}]$ in the equilibrium condition (9), and then the new equilibrium condition

is given by

$$\omega_T^2\bar{x}\boldsymbol{e}_1=\frac{\mu}{r^3}\bar{\boldsymbol{r}}-\frac{3\mu}{2r^5}\Big\{\Big[\tau_0\left(1-5\bar{z}^2\right)-10\tau_2\bar{x}^2+5\bar{\boldsymbol{r}}^{\mathrm{T}}\boldsymbol{A}\left(\boldsymbol{I}/m\right)\boldsymbol{A}^{\mathrm{T}}\bar{\boldsymbol{r}}-\mathrm{tr}\left(\boldsymbol{I}/m\right)\Big]\bar{\boldsymbol{r}}+2\tau_0\bar{z}\boldsymbol{e}_3+4\tau_2\bar{x}\boldsymbol{e}_1-2\boldsymbol{A}\left(\boldsymbol{I}/m\right)\boldsymbol{A}^{\mathrm{T}}\bar{\boldsymbol{r}}\Big\} \tag{11}$$

4 Iteration methods

Although in-plane non-equatorial equilibrium points can be solved based on Eq. (11) by using a numerical method, such as fsolve in the software MATLAB, in most cases it is difficult to have a satisfying result due to the significant nonlinearity and high sensitivity of the system. Therefore, we develop two iteration methods based on the equilibrium condition to determine equilibrium points with a higher accuracy.

4.1 Iteration method I

We first assume that the orbit radius r is already known, and then the equilibrium condition in Eq. (11) can be rearranged as

$$\frac{\mu}{r^3}\bar{\boldsymbol{r}}-\frac{3\mu}{2r^5}\Big\{\Big[\tau_0\left(1-5\bar{z}^2\right)-10\tau_2\bar{x}^2+5\bar{\boldsymbol{r}}^{\mathrm{T}}\boldsymbol{A}\left(\boldsymbol{I}/m\right)\boldsymbol{A}^{\mathrm{T}}\bar{\boldsymbol{r}}-\mathrm{tr}\left(\boldsymbol{I}/m\right)\Big]\bar{\boldsymbol{r}}+2\tau_0\bar{z}\boldsymbol{e}_3+\left[4\tau_2+2\omega_T^2r^5/(3\mu)\right]\bar{x}\boldsymbol{e}_1-2\boldsymbol{A}\left(\boldsymbol{I}/m\right)\boldsymbol{A}^{\mathrm{T}}\bar{\boldsymbol{r}}\Big\}=0 \tag{12}$$

which requires that $\tau_0\bar{z}\boldsymbol{e}_3+\left[2\tau_2+\omega_T^2r^5/(3\mu)\right]\bar{x}\boldsymbol{e}_1-\boldsymbol{A}\left(\boldsymbol{I}/m\right)\boldsymbol{A}^{\mathrm{T}}\bar{\boldsymbol{r}}$ is parallel to the position vector $\bar{\boldsymbol{r}}$. Notice that the position vector $\bar{\boldsymbol{r}}$ is within the $\boldsymbol{u}$–$\boldsymbol{w}$ plane spanned by $\boldsymbol{e}_1$ and $\boldsymbol{e}_3$, and therefore, $\boldsymbol{A}\left(\boldsymbol{I}/m\right)\boldsymbol{A}^{\mathrm{T}}\bar{\boldsymbol{r}}$ should also be within the $\boldsymbol{u}$–$\boldsymbol{w}$ plane. Then, we can know that the $\boldsymbol{u}$–$\boldsymbol{w}$ plane is the principal plane of the spacecraft's inertia tensor $\boldsymbol{A}\left(\boldsymbol{I}/m\right)\boldsymbol{A}^{\mathrm{T}}$ expressed in the asteroid's frame S_{P}. That is to say, one of the $\boldsymbol{i}$–$\boldsymbol{j}$ plane, $\boldsymbol{j}$–$\boldsymbol{k}$ plane, and $\boldsymbol{i}$–$\boldsymbol{k}$ plane of the spacecraft is within the $\boldsymbol{u}$–$\boldsymbol{w}$ plane of the asteroid. Without loss of generality, we assume that the $\boldsymbol{i}$–$\boldsymbol{k}$ plane is within the $\boldsymbol{u}$–$\boldsymbol{w}$ plane of the asteroid, and the unit vectors $\boldsymbol{j}$ and $\boldsymbol{v}$ have the same direction. Other cases can be converted into this case easily by changing the arrangement of axes of the spacecraft's body-fixed frame S_{B}. That is to say, the relative attitude of spacecraft with respect to the asteroid is just a single axis rotation around the $\boldsymbol{v}$-axis, i.e.,

$$\boldsymbol{A}=\begin{bmatrix}\cos\theta & 0 & \sin\theta\\ 0 & 1 & 0\\ -\sin\theta & 0 & \cos\theta\end{bmatrix} \tag{13}$$

where θ is the rotational angle. Therefore, we have

$$\boldsymbol{A}\left(\boldsymbol{I}/m\right)\boldsymbol{A}^{\mathrm{T}}=\begin{bmatrix}\cos^2\theta I_{xx}/m+\sin^2\theta I_{zz}/m & 0 & \sin\theta\cos\theta\left(I_{zz}/m-I_{xx}/m\right)\\ 0 & I_{yy}/m & 0\\ \sin\theta\cos\theta\left(I_{zz}/m-I_{xx}/m\right) & 0 & \sin^2\theta I_{xx}/m+\cos^2\theta I_{zz}/m\end{bmatrix} \tag{14}$$

and

$$\tau_0\bar{z}\boldsymbol{e}_3+\left[2\tau_2+\omega_T^2r^5/(3\mu)\right]\bar{x}\boldsymbol{e}_1-\boldsymbol{A}\left(\boldsymbol{I}/m\right)\boldsymbol{A}^{\mathrm{T}}\bar{\boldsymbol{r}}=\begin{bmatrix}-\left[\cos^2\theta I_{xx}/m+\sin^2\theta I_{zz}/m-\omega_T^2r^5/(3\mu)-2\tau_2\right]\bar{x}-\sin\theta\cos\theta\left(I_{zz}/m-I_{xx}/m\right)\bar{z}\\ 0\\ -\sin\theta\cos\theta\left(I_{zz}/m-I_{xx}/m\right)\bar{x}-\left(\sin^2\theta I_{xx}/m+\cos^2\theta I_{zz}/m-\tau_0\right)\bar{z}\end{bmatrix} \tag{15}$$

Then, the condition that $\tau_0\bar{z}\boldsymbol{e}_3+\left[2\tau_2+\omega_T^2r^5/(3\mu)\right]\bar{x}\boldsymbol{e}_1-\boldsymbol{A}\left(\boldsymbol{I}/m\right)\boldsymbol{A}^{\mathrm{T}}\bar{\boldsymbol{r}}$ is parallel to the position vector $\bar{r}$ is equivalent to

$$\frac{\left\{\left[\cos^2\theta I_{xx}/m+\sin^2\theta I_{zz}/m-\omega_T^2r^5/(3\mu)-2\tau_2\right]\bar{x}+\sin\theta\cos\theta\left(I_{zz}/m-I_{xx}/m\right)\bar{z}\right\}}{\left[\sin\theta\cos\theta\left(I_{zz}/m-I_{xx}/m\right)\bar{x}+\left(\sin^2\theta I_{xx}/m+\cos^2\theta I_{zz}/m-\tau_0\right)\bar{z}\right]}=\frac{\bar{x}}{\bar{z}} \tag{16}$$

which can be further simplified as

$$\frac{\left\{\left[\cos^2\theta+\sin^2\theta I_{zz}/I_{xx}-2\omega_T^2r^5/\left(3\mu\rho^2\right)-4\tau_2/\rho^2\right]\bar{x}+\sin\theta\cos\theta\left(I_{zz}/I_{xx}-1\right)\bar{z}\right\}}{\left[\sin\theta\cos\theta\left(I_{zz}/I_{xx}-1\right)\bar{x}+\left(\sin^2\theta+\cos^2\theta I_{zz}/I_{xx}-2\tau_0/\rho^2\right)\bar{z}\right]}=\frac{\bar{x}}{\bar{z}} \tag{17}$$

We can see that Eq. (17) is affected by the mass distribution parameter I_{zz}/I_{xx}, the characteristic dimension ρ, and the attitude angle θ of the spacecraft.

These parameters are all introduced into the system by the GOACP $\boldsymbol{\alpha}_{\mathrm{OAC}}$.

After some rearrangements, Eq. (17) can be simplified as

$$\begin{aligned}&\sin\theta\cos\theta\left(I_{zz}/I_{xx}-1\right)\left(\bar{z}^2-\bar{x}^2\right)\\&\quad+\left[\left(\cos^2\theta-\sin^2\theta\right)\left(1-I_{zz}/I_{xx}\right)-2\omega_T^2r^5/\left(3\mu\rho^2\right)\right.\\&\quad\left.-4C_{22}a_e^2/\rho^2+2C_{20}a_e^2/\rho^2\right]\bar{x}\bar{z}=0\end{aligned}\tag{18}$$

By using the relation $\bar{x}^2+\bar{z}^2=1$, Eq. (18) can be written as

$$\bar{x}^4-\bar{x}^2+c=0\tag{19}$$

where

$$\begin{aligned}c=&\sin^2\theta\cos^2\theta\left(1-\frac{I_{zz}}{I_{xx}}\right)^2\Bigg/\left\{4\sin^2\theta\cos^2\theta\left(1-\frac{I_{zz}}{I_{xx}}\right)^2\right.\\&+\left[\left(\cos^2\theta-\sin^2\theta\right)\left(1-\frac{I_{zz}}{I_{xx}}\right)-\frac{2\omega_T^2r^5}{3\mu\rho^2}\right.\\&\left.\left.-\frac{4C_{22}a_e^2}{\rho^2}+\frac{2C_{20}a_e^2}{\rho^2}\right]^2\right\}>0\end{aligned}\tag{20}$$

Therefore, we have

$$\bar{x}^2=\frac{1\pm\sqrt{1-4c}}{2}\tag{21}$$

which contains four solutions: if the terms $\sin\theta\cos\theta\cdot\left(I_{zz}/I_{xx}-1\right)$ and $\left(\cos^2\theta-\sin^2\theta\right)\left(1-I_{zz}/I_{xx}\right)-2\omega_T^2r^5/\left(3\mu\rho^2\right)-4C_{22}a_e^2/\rho^2+2C_{20}a_e^2/\rho^2$ in Eq. (18) have the same sign, $\bar{z}^2-\bar{x}^2$ and $\bar{x}\bar{z}$ will have the opposite signs, and then

$$\begin{aligned}&\bar{x}=\pm\sqrt{\frac{1+\sqrt{1-4c}}{2}},\ \bar{z}=\pm\sqrt{\frac{1-\sqrt{1-4c}}{2}}\\&\text{or}\quad\bar{x}=\pm\sqrt{\frac{1-\sqrt{1-4c}}{2}},\ \bar{z}=\mp\sqrt{\frac{1+\sqrt{1-4c}}{2}}\end{aligned}\tag{22}$$

if the terms $\sin\theta\cos\theta\left(I_{zz}/I_{xx}-1\right)$ and $\left(\cos^2\theta-\sin^2\theta\right)\left(1-I_{zz}/I_{xx}\right)-2\omega_T^2r^5/\left(3\mu\rho^2\right)-4C_{22}a_e^2/\rho^2+2C_{20}a_e^2/\rho^2$ in Eq. (18) have the opposite signs, $\bar{z}^2-\bar{x}^2$ and $\bar{x}\bar{z}$ will have the same sign, and then

$$\begin{aligned}&\bar{x}=\pm\sqrt{\frac{1+\sqrt{1-4c}}{2}},\ \bar{z}=\mp\sqrt{\frac{1-\sqrt{1-4c}}{2}}\\&\text{or}\quad\bar{x}=\pm\sqrt{\frac{1-\sqrt{1-4c}}{2}},\ \bar{z}=\pm\sqrt{\frac{1+\sqrt{1-4c}}{2}}\end{aligned}\tag{23}$$

These four solutions are located in four quadrants of the asteroid's $\boldsymbol{u}$–$\boldsymbol{w}$ plane, respectively. Due to the system's symmetry, equilibrium points in the first and third quadrants are symmetrical with respect to the asteroid center. The equilibrium points in the second and fourth quadrants are symmetrical as well. These have also been shown by Eqs. (22) and (23): the first and second solutions have the opposite signs, and the third and fourth solutions have the opposite signs, too

With Eqs. (20), (22), and (23), we can obtain the position vector $\bar{\boldsymbol{r}}=[\bar{x},\ 0,\ \bar{z}]$, i.e., the latitude of in-plane non-equatorial equilibrium points. Then, according to Eq. (12), the orbit radius of the equilibrium point can be calculated by

$$\begin{aligned}&\frac{\mu}{r^3}-\frac{3\mu}{2r^5}\left[\tau_0\left(1-5\bar{z}^2\right)-10\tau_2\bar{x}^2+5\bar{\boldsymbol{r}}^{\mathrm{T}}\boldsymbol{A}\left(\boldsymbol{I}/m\right)\boldsymbol{A}^{\mathrm{T}}\bar{\boldsymbol{r}}\right.\\&\quad\left.-\mathrm{tr}\left(\boldsymbol{I}/m\right)+a\right]=0\end{aligned}\tag{24}$$

where $a\bar{\boldsymbol{r}}=2\tau_0\bar{z}\boldsymbol{e}_3+\left[4\tau_2+2\omega_T^2r^5\ /\ (3\mu)\right]\bar{x}\boldsymbol{e}_1-2\boldsymbol{A}\left(\boldsymbol{I}/m\right)\boldsymbol{A}^{\mathrm{T}}\bar{\boldsymbol{r}}$, that is,

$$r=\sqrt{\frac{3}{2}\left[\tau_0\left(1-5\bar{z}^2\right)-10\tau_2\bar{x}^2+5\bar{\boldsymbol{r}}^{\mathrm{T}}\boldsymbol{A}\left(\frac{\boldsymbol{I}}{m}\right)\boldsymbol{A}^{\mathrm{T}}\bar{\boldsymbol{r}}-\mathrm{tr}\left(\frac{\boldsymbol{I}}{m}\right)+a\right]}\tag{25}$$

Equation (25) for the orbit radius r needs the value of a, but, unfortunately, the calculation of a needs r first. Therefore, here we have to use an iteration method by repeating the procedure given by Eqs. (12)–(24) with an initial guess of r until r converges. We can first calculate the equilibrium points in the case of $\theta=0$, which is simpler. Then, we calculate the equilibrium points as θ increases gradually from 0 to π with a small step size. The value of r for last value of θ can be used as the initial guess for the current value of θ. Notice that the considered range of θ is $0\leqslant\theta\leqslant\pi$, since $\pi\leqslant\theta\leqslant2\pi$ is actually the same case with $0\leqslant\theta\leqslant\pi$ because of the symmetry of spacecraft's inertia tensor. With this method, we can obtain the loci of non-equatorial equilibrium points in the $\boldsymbol{u}$–$\boldsymbol{w}$ plane with respect to θ.

4.2 Iteration method II

The iteration method I in Section 4.1 begins with an initial guess of the orbit radius r, then calculates $\bar{x}$ and $\bar{z}$, and finally obtains a new value of r. However, in the calculation of some equilibrium points, r cannot converge. Therefore, a second iteration method, which begins with an initial guess of $\bar{x}$ and $\bar{z}$, then calculates r, and finally obtains new values for $\bar{x}$ and $\bar{z}$, is needed. The procedure of iteration method II will be given in

the following. Provided an initial guess of $\bar{x}$ and $\bar{z}$, according to Eq. (18), the orbit radius r can be given by

$$r = \Big(\frac{3\mu\rho^2}{2\omega_T^2 \bar{x}\bar{z}} \{ \sin\theta\cos\theta \left(I_{zz}/I_{xx} - 1\right) \left(\bar{z}^2 - \bar{x}^2\right) + \left[\left(\cos^2\theta - \sin^2\theta\right) \left(1 - I_{zz}/I_{xx}\right) - 4C_{22}a_e^2/\rho^2 + 2C_{20}a_e^2/\rho^2 \right] \bar{x}\bar{z} \} \Big)^{1/5} \quad (26)$$

Then the equilibrium condition in Eq. (12) can be written as

$$\frac{\mu}{r^3} - \frac{3\mu}{2r^5} \left[\tau_0 \left(1 - 5\bar{z}^2\right) - 10\tau_2\bar{x}^2 + 5\bar{\boldsymbol{r}}^{\mathrm{T}} \boldsymbol{A} \left(\boldsymbol{I}/m\right) \boldsymbol{A}^{\mathrm{T}} \bar{\boldsymbol{r}} - \mathrm{tr}\left(\boldsymbol{I}/m\right) + a \right] = 0 \quad (27)$$

where $a\bar{\boldsymbol{r}} = 2\tau_0\bar{z}\boldsymbol{e}_3 + \left[4\tau_2 + 2\omega_T^2 r^5 \,/\, (3\mu)\right] \bar{x}\boldsymbol{e}_1 - 2\boldsymbol{A}\left(\boldsymbol{I}/m\right)\boldsymbol{A}^{\mathrm{T}}\bar{\boldsymbol{r}}$. Equation (27) can be written as

$$\begin{aligned} &5\left(\cos^2\theta I_{xx}/m + \sin^2\theta I_{zz}/m - 2\tau_2\right)\bar{x}^2 \\ &+ 10\sin\theta\cos\theta\left(I_{zz}/m - I_{xx}/m\right)\bar{x}\bar{z} \\ &+ 5\left(\sin^2\theta I_{xx}/m + \cos^2\theta I_{zz}/m - \tau_0\right)\bar{z}^2 \\ &- \frac{2}{3}r^2 + \tau_0 - \mathrm{tr}\left(\boldsymbol{I}/m\right) + a = 0 \end{aligned} \quad (28)$$

By using Eq. (28) and the relation $\bar{x}^2 + \bar{z}^2 = 1$, the new value of $\bar{x}$ and $\bar{z}$ can be calculated. Repeat the above procedure until $\bar{x}$ and $\bar{z}$ converge.

Similar to iteration method I in Section 4.1, we first calculate equilibrium points in the case of $\theta = 0$, and then we calculate equilibrium points as θ increases from 0 to π with a small step size. The values of $\bar{x}$ and $\bar{z}$ corresponding to last value of θ can be used as the initial guess for current value of θ.

5 In-plane non-equatorial equilibrium points

5.1 In-plane non-equatorial equilibrium points for $\theta = 0$

In the case of $\theta = 0$, Eq. (17) can be written as

$$\frac{\left[1 - 2\omega_T^2 r^5/\left(3\mu\rho^2\right) - 4\tau_2/\rho^2\right]\bar{x}}{\left(I_{zz}/I_{xx} - 2\tau_0/\rho^2\right)\bar{z}} = \frac{\bar{x}}{\bar{z}} \quad (29)$$

which implies that $\bar{x} = 0$, or $\bar{z} = 0$, or $1 - 2\omega_T^2 r^5/\left(3\mu\rho^2\right) - 4\tau_2/\rho^2 = I_{zz}/I_{xx} - 2\tau_0/\rho^2$

5.1.1 $\bar{x} = 0$, $\bar{z} = \pm 1$

In this case, the spacecraft is located on the $\boldsymbol{w}$-axis of the asteroid, and the equilibrium condition (11) can be written as

$$\frac{\mu}{r^3} - \frac{3\mu}{2r^5}\left(-2\tau_0 + 2I_{zz}/m - I_{xx}/m - I_{yy}/m\right) = 0 \quad (30)$$

which can be simplified as

$$r = \sqrt{\frac{3}{2}\left(-2\tau_0 + 2I_{zz}/m - I_{xx}/m - I_{yy}/m\right)} \quad (31)$$

If the GOACP $\boldsymbol{\alpha}_{\mathrm{OAC}}$ is neglected, these two polar equilibrium points will be degenerated to be the classical polar equilibrium points in the point-mass orbital model, the orbit radius r of which is given by

$$r = \sqrt{-3\tau_0} = a_e\sqrt{-3C_{20}} \quad (32)$$

Equation (32) implies that only in the case of $C_{20} < -1/3$ the two polar equilibrium points can be located above the asteroid's surface, but $C_{20} < -1/3$ is unrealistic in the real physics. Besides, the equilibrium points are located very close to the asteroid's surface, and the precision of the approximation by harmonic coefficients C_{20} and C_{22} are questionable. Therefore, these polar equilibrium points are unrealistic, and they were not considered by Howard [26].

5.1.2 $\bar{z} = 0$, $\bar{x} = \pm 1$

In this case, the spacecraft is located on the $\boldsymbol{u}$-axis of the asteroid, and then the equilibrium condition (11) can be written as

$$\omega_T^2 = \frac{\mu}{r^3} - \frac{3\mu}{2r^5}\left(\tau_0 - 6\tau_2 + 2I_{xx}/m - I_{yy}/m - I_{zz}/m\right) \quad (33)$$

by using which the orbit radius r can be determined. The two equilibria given by Eq. (33) are actually the on-axis equatorial equilibrium points given previously by Wang and Xu [24].

If the GOACP $\boldsymbol{\alpha}_{\mathrm{OAC}}$ is neglected, these two on-axis equilibrium points will be degenerated to be the classical equatorial equilibrium points in the point-mass orbital model in Howard [26], the orbit radius r of which is given by

$$\omega_T^2 = \frac{\mu}{r^3} - \frac{3\mu}{2r^5}\left(\tau_0 - 6\tau_2\right) \quad (34)$$

In our study, due to the GOACP $\boldsymbol{\alpha}_{\mathrm{OAC}}$, the orbit radius r given by Eq. (33) is different from the point-mass orbital model Eq. (34). As the attitude angle θ changes from 0 to π, these two equilibria, which can be calculated by the iteration method, will move off the $\boldsymbol{u}$-axis but within the $\boldsymbol{u}$–$\boldsymbol{w}$ plane.

5.1.3 $1 - 2\omega_T^2 r^5/(3\mu\rho^2) - 4\tau_2/\rho^2 = I_{zz}/I_{xx} - 2\tau_0/\rho^2$

If the GOACP $\boldsymbol{\alpha}_{\mathrm{OAC}}$ is neglected, this case will be

degenerated to be the classical non-equatorial equilibrium points in Howard [26], that is, $2\tau_2+\omega_T^2 r^5/(3\mu)=\tau_0$. Then we have

$$r=\sqrt[5]{3\mu\left(\tau_0-2\tau_2\right)/\omega_T^2} \tag{35}$$

Since τ_0 is negative, $2\tau_2+\omega_T^2 r^5/(3\mu)=\tau_0$ means that τ_2 is also negative and then the $\boldsymbol{u}$–$\boldsymbol{w}$ plane is the asteroid's principal plane spanned by $\boldsymbol{w}$-axis and the shorter equatorial principal axis. This is consistent with the conclusion by Howard [26] that the classical non-equatorial equilibrium points without GOACP can only exist within the principal plane spanned by $\boldsymbol{w}$-axis and the shorter equatorial principal axis.

In this case, the equilibrium condition (11) is simpler

$$\begin{aligned}\omega_T^2\bar{x}\boldsymbol{e}_1=&\frac{\mu}{r^3}\bar{\boldsymbol{r}}-\frac{3\mu}{2r^5}\left\{\left[\tau_0\left(1-5\bar{z}^2\right)-10\tau_2\bar{x}^2\right]\bar{\boldsymbol{r}}\right.\\&\left.+2\tau_0\bar{z}\boldsymbol{e}_3+4\tau_2\bar{x}\boldsymbol{e}_1\right\}\end{aligned} \tag{36}$$

which can be written as follows by using Eq. (35):

$$\frac{\mu}{r^3}-\frac{3\mu}{2r^5}\left[\tau_0\left(3-5\bar{z}^2\right)-10\tau_2\bar{x}^2\right]=0 \tag{37}$$

By using the relation $\bar{x}^2+\bar{z}^2=1$, Eq. (37) has four solutions:

$$\begin{aligned}&\bar{x}=\sqrt{\frac{2r^2+6\tau_0}{15\left(\tau_0-2\tau_2\right)}},\ \bar{z}=\mp\sqrt{\frac{9\tau_0-30\tau_2-2r^2}{15\left(\tau_0-2\tau_2\right)}}\\ \text{or}\ \ &\bar{x}=-\sqrt{\frac{2r^2+6\tau_0}{15\left(\tau_0-2\tau_2\right)}},\ \bar{z}=\pm\sqrt{\frac{9\tau_0-30\tau_2-2r^2}{15\left(\tau_0-2\tau_2\right)}}\end{aligned} \tag{38}$$

where the orbit radius r is given by Eq. (35). The classical non-equatorial equilibrium points in Eq. (38) appear as a quadruplet, which have the same orbital radius and the same absolute value of latitude. According to Eqs. (35) and (38), these classical non-equatorial equilibrium points can exist when

$$\tau_0>2\tau_2\quad\text{and}\quad 0\leqslant\frac{2r^2+6\tau_0}{15\left(\tau_0-2\tau_2\right)}\leqslant 1 \tag{39}$$

In our study, when $\theta=0$, due to the GOACP $\boldsymbol{\alpha}_{\mathrm{OAC}}$, the relation in the classical point-mass orbital model $2\tau_2+\omega_T^2 r^5/(3\mu)=\tau_0$ will be changed to $1-2\omega_T^2 r^5/\left(3\mu\rho^2\right)-4\tau_2/\rho^2=I_{zz}/I_{xx}-2\tau_0/\rho^2$, as shown by Eq. (29). Then, the orbit radius r in Eq. (35) will also be changed as

$$r=\sqrt[5]{\frac{3\mu}{2\omega_T^2}\left[\rho^2\left(1-\frac{I_{zz}}{I_{xx}}\right)+2\tau_0-4\tau_2\right]} \tag{40}$$

In this case, the equilibrium condition (11) will be

$$\begin{aligned}\omega_T^2\bar{x}\boldsymbol{e}_1=&\frac{\mu}{r^3}\bar{\boldsymbol{r}}-\frac{3\mu}{2r^5}\left\{\left[\tau_0\left(1-5\bar{z}^2\right)-10\tau_2\bar{x}^2\right.\right.\\&\left.+5\left(\bar{x}^2I_{xx}/m+\bar{z}^2I_{zz}/m\right)-\mathrm{tr}\left(\boldsymbol{I}/m\right)\right]\bar{\boldsymbol{r}}\\&+2\tau_0\bar{z}\boldsymbol{e}_3+4\tau_2\bar{x}\boldsymbol{e}_1-2\left(\bar{x}I_{xx}/m\boldsymbol{e}_1\right.\\&\left.\left.+\ \bar{z}I_{zz}/m\boldsymbol{e}_3\right)\right\}\end{aligned} \tag{41}$$

which can be written as follows by using $1-2\omega_T^2 r^5/\left(3\mu\rho^2\right)-4\tau_2/\rho^2=I_{zz}/I_{xx}-2\tau_0/\rho^2$

$$\begin{aligned}&5\left(I_{xx}/m-2\tau_2\right)\bar{x}^2+5\left(I_{zz}/m-\tau_0\right)\bar{z}^2\\&=2r^2/3+\mathrm{tr}\left(\boldsymbol{I}/m\right)+2I_{zz}/m-3\tau_0\end{aligned} \tag{42}$$

By using the relation $\bar{x}^2+\bar{z}^2=1$, Eq. (42) has four solutions:

$$\begin{aligned}&\bar{x}=\sqrt{\frac{2r^2/3+2\tau_0+\mathrm{tr}\left(\boldsymbol{I}/m\right)-3I_{zz}/m}{5\left(I_{xx}/m-I_{zz}/m+\tau_0-2\tau_2\right)}},\\&\bar{z}=\pm\sqrt{\frac{3\tau_0-10\tau_2-2r^2/3+5I_{xx}/m-2I_{zz}/m-\mathrm{tr}\left(\boldsymbol{I}/m\right)}{5\left(I_{xx}/m-I_{zz}/m+\tau_0-2\tau_2\right)}}\\\text{or}\ \ &\bar{x}=-\sqrt{\frac{2r^2/3+2\tau_0+\mathrm{tr}\left(\boldsymbol{I}/m\right)-3I_{zz}/m}{5\left(I_{xx}/m-I_{zz}/m+\tau_0-2\tau_2\right)}},\\&\bar{z}=\pm\sqrt{\frac{3\tau_0-10\tau_2-2r^2/3+5I_{xx}/m-2I_{zz}/m-\mathrm{tr}\left(\boldsymbol{I}/m\right)}{5\left(I_{xx}/m-I_{zz}/m+\tau_0-2\tau_2\right)}}\end{aligned} \tag{43}$$

According to Eqs. (40) and (43), these equilibrium points can exist when

$$\begin{aligned}&\rho^2\left(1-\frac{I_{zz}}{I_{xx}}\right)+2\tau_0-4\tau_2>0\quad\text{and}\\&0\leqslant\frac{2r^2/3+2\tau_0+\mathrm{tr}\left(\boldsymbol{I}/m\right)-3I_{zz}/m}{5\left(I_{xx}/m-I_{zz}/m+\tau_0-2\tau_2\right)}\leqslant 1\end{aligned} \tag{44}$$

The differences between the classical non-equatorial equilibrium points described by Eqs. (35) and (38), and the non-equatorial equilibrium points described by Eqs. (40) and (43) are due to the GOACP with $\theta=0$. As the attitude angle θ changes from 0 to π, the four equilibria given by Eqs. (40) and (43), which can be calculated by the iteration method, will move within the $\boldsymbol{u}$–$\boldsymbol{w}$ plane.

5.2 In-plane non-equatorial equilibrium points for $0<\theta<\pi$

Using equilibrium points in the case of $\theta=0$ given in

Section 5.1 as the initial guess, we can calculate equilibrium points for $0 < \theta < \pi$ through the following three methods:

(a) Solving the equilibrium condition, i.e., the algebra equation system (11), by using a numerical method, such as fsolve in the software MATLAB.

(b) Iteration method I in Section 4.1.

(c) Iteration method II in Section 4.2.

Actually, all these three methods rely on the iteration procedure, and each of them needs an initial guess. With the equilibrium points in the case of $\theta = 0$ already obtained in Section 5.1, we can calculate equilibrium points as θ increases gradually from 0 to π with a small step size.

According to the results in Section 5.1, by abandoning the unrealistic equilibrium points in Section 5.1.1, the in-plane non-equatorial equilibrium points can be divided into two families:

(a) The first family is near the asteroid's $\boldsymbol{u}$-axis and emerges from equilibrium points in Section 5.1.2 as θ increases from 0 to π. This family is the generalization of classical equatorial on-axis equilibrium points without GOACP in Eq. (34).

(b) The second family is near the classical non-equatorial equilibrium points given by Howard [26] and emerges from equilibrium points in Section 5.1.3 as θ increases from 0 to π. This family is the generalization of classical non-equatorial equilibrium points without GOACP in Eqs. (35) and (38).

During the calculation, we have found that due to the different local properties of different families, the method (a) is more suitable for solving the first family and the method (c) is more suitable for solving the second family.

5.2.1 *First family of non-equatorial equilibrium points*

We give some calculation examples of in-plane non-equatorial equilibrium points and to investigate the effect of GOACP $\boldsymbol{\alpha}_{\mathrm{OAC}}$ on their locations. First, we focus on the first family.

The parameters of the asteroid are chosen to be the same as the example asteroid in Wang and Xu [24]:

$$\begin{aligned} &\mu = 5\ \mathrm{m}^3/\mathrm{s}^2, \quad C_{20} = -0.12, \quad C_{22} = 0.01, \\ &a_e = 250\ \mathrm{m}, \quad \omega_T = 2.9089 \times 10^{-4}\ \mathrm{s}^{-1} \end{aligned} \tag{45}$$

which has a similar size with target of OSIRIS-REx mission, asteroid 101955 Bennu (provisional designation 1999 RQ_{36}), but has larger values for C_{20} and C_{22} than the approximate values of Bennu. The period of the asteroid's uniform rotation is 6 h.

The mass distribution of spacecraft is set to be

$$I_{xx} : I_{yy} : I_{zz} = 1.5 : 1.2 : 1 \tag{46}$$

which is a common case in space engineering. As for the spacecraft's characteristic dimension ρ, we choose five different values as follows:

$$\rho = 0\ \mathrm{m}, \quad \rho = 2\ \mathrm{m}, \quad \rho = 50\ \mathrm{m}, \quad \rho = 100\ \mathrm{m}, \quad \rho = 160\ \mathrm{m} \tag{47}$$

where $\rho = 0$ m corresponds to the classical point-mass orbital dynamics without GOACP. As stated in Wang and Xu [24], $\rho = 2$ m corresponds to a general asteroid probe, and the maximum $\rho = 160$ m corresponds to large spacecraft in future asteroid missions, such as a big gravity tractor in asteroid deflection missions, or the mothership in asteroid resource exploitation. The large ρ seems to be extreme in the current deep space missions, but perhaps will be common in future missions.

By using the method (a), fsolve in the software MATLAB, the first family of non-equatorial equilibrium points can be obtained through the iteration procedure with equilibrium points in Section 5.1.2 as initial guesses. We then plot the loci of the first family of non-equatorial equilibrium points in the longitudinal principal plane, i.e., the $\boldsymbol{u}$–$\boldsymbol{w}$ plane of the asteroid, with respect to the spacecraft's attitude angle θ in the cases of different ρ. The loci are given in Figs. 2–6, respectively.

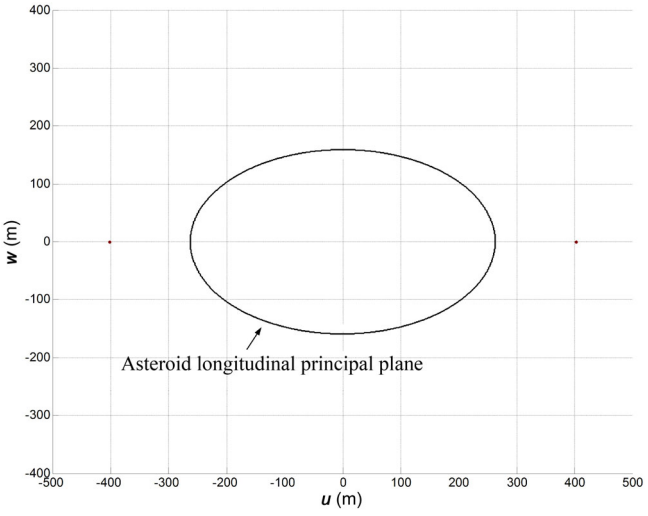

Fig. 2 Classical equilibrium points in point-mass orbital dynamics without GOACP.

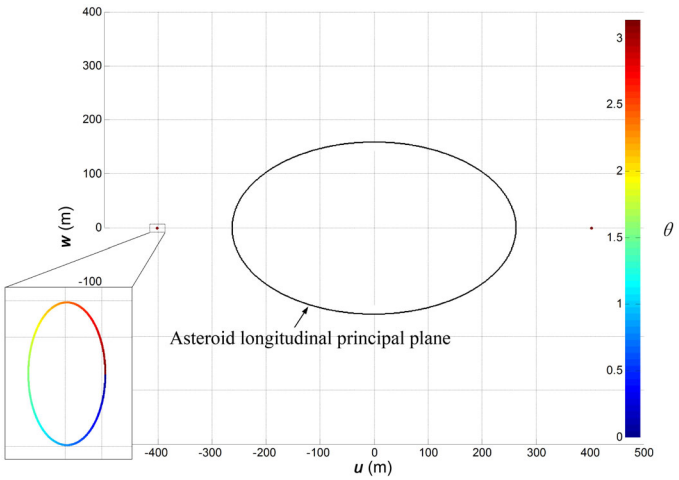

Fig. 3 Loci of the first family of non-equatorial equilibrium points in the case of $\rho = 2$ m.

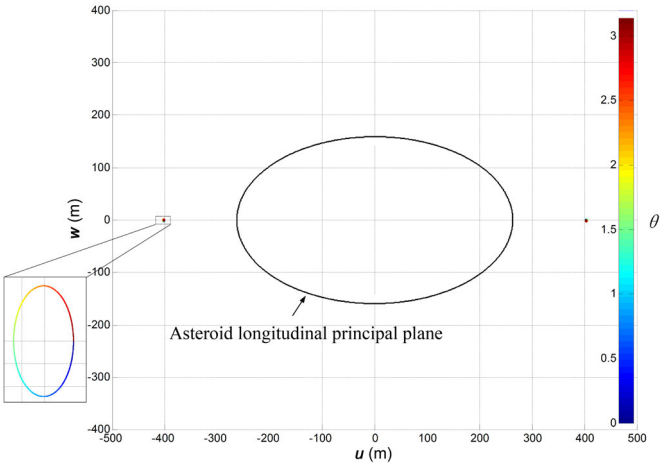

Fig. 4 Loci of the first family of non-equatorial equilibrium points in the case of $\rho = 50$ m.

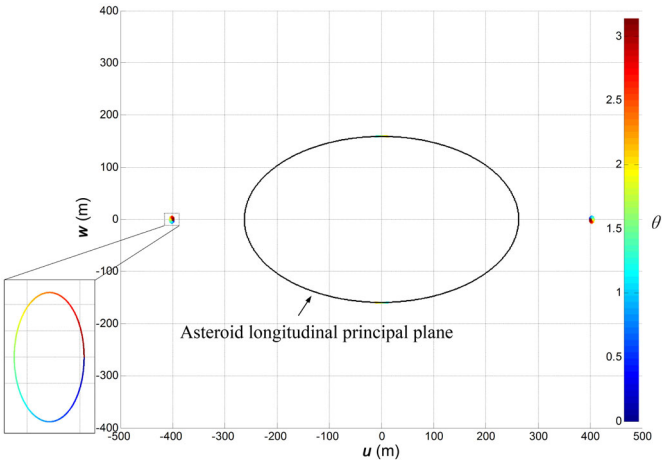

Fig. 5 Loci of the first family of non-equatorial equilibrium points in the case of $\rho = 100$ m.

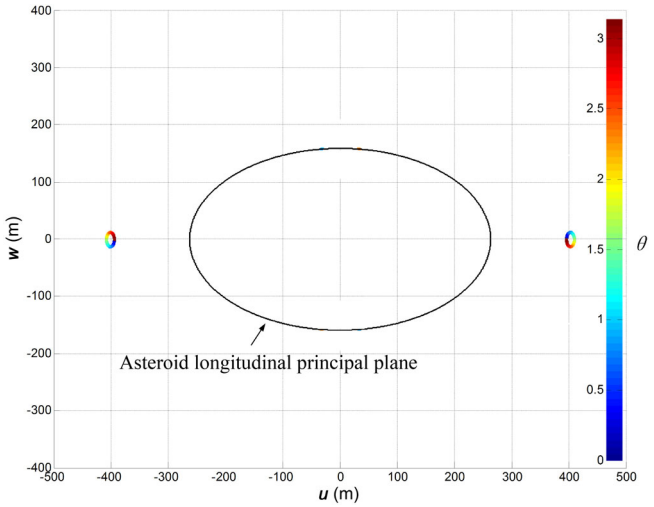

Fig. 6 Loci of the first family of non-equatorial equilibrium points in the case of $\rho = 160$ m.

5.2.2 Discussions on the first family

In Figs. 2–6 we have calculated the first family of non-equatorial equilibrium points only in the $\boldsymbol{u}$–$\boldsymbol{w}$ plane of the asteroid. Actually, in the $\boldsymbol{v}$–$\boldsymbol{w}$ plane, the first family, which is similar to that in the $\boldsymbol{u}$–$\boldsymbol{w}$ plane in Figs. 2–6, also exists and can be calculated with the same method. Therefore, without loss of generality, we will discuss the first family only in the $\boldsymbol{u}$–$\boldsymbol{w}$ plane.

According to Figs. 2–6, some important conclusions about the first family of non-equatorial equilibrium points can be drawn:

(a) The first family refers ton on-equatorial equilibrium points near the asteroid's $\boldsymbol{u}$-axis in Figs. 3–6, which is the generalization of classical on-axis equilibrium points without GOACP given by Eq. (34) and Fig. 2.

(b) All the loci are symmetrical with respect to the asteroid's principal axes $\boldsymbol{u}$-axis and $\boldsymbol{w}$-axis due to symmetries of mass distributions of the asteroid and the spacecraft. Besides, for a given value of attitude angle θ, non-equatorial equilibrium points are symmetrical with respect to the asteroid's center.

(c) As ρ increases, the effect of GOACP $\boldsymbol{\alpha}_{\mathrm{OAC}}$ becomes more significant, and the shift of the first family from the asteroid's principal axis $\boldsymbol{u}$-axis gets larger.

When $\rho = 2$ m, the effect of GOACP $\boldsymbol{\alpha}_{\mathrm{OAC}}$ is weak. The system is close to the classical orbital dynamics without $\boldsymbol{\alpha}_{\mathrm{OAC}}$, and the non-equatorial equilibrium points are close to the classical ones without $\boldsymbol{\alpha}_{\mathrm{OAC}}$, as shown by Figs. 2 and 3.

In Figs. 3–6, as ρ increases to 160 m, the loci of the equilibrium points expand from the vicinity of the

classical ones without $\boldsymbol{\alpha}_{\mathrm{OAC}}$, and the maximum shift from the asteroid's principal axes gets larger.

(d) As shown by Figs. 3–6, the loci of non-equatorial equilibrium points are two closed curves around the classical ones without $\boldsymbol{\alpha}_{\mathrm{OAC}}$. For a given value of θ, there exist two non-equatorial equilibrium points. These two equilibrium points are located on the two closed curves, respectively, and are symmetrical with respect to the asteroid's center.

With the attitude angle θ changing from 0 to π, the non-equatorial equilibrium point will move along the closed curve for one cycle. When θ changes from 0 to $\pi/2$, the non-equatorial equilibrium point will move off the asteroid's principal axis, and after reaching the maximum shift it will move back towards, and finally return to, the asteroid's principal axis when $\theta = \pi/2$. As θ changes further from $\pi/2$ to π, the non-equatorial equilibrium point will move off the asteroid's principal axis in the opposite direction. The locus between $\theta = \pi/2$ and $\theta = \pi$ and that between $\theta = 0$ and $\theta = \pi/2$ are symmetrical with respect to the asteroid's principal axis. The equilibrium point will return to the starting point $\theta = 0$ on the asteroid's principal axis when $\theta = \pi$. When $\theta = 0$ (π) and $\theta = \pi/2$, the non-equatorial equilibrium points are on the asteroid's $\boldsymbol{u}$-axis.

(e) Compared with classical equilibrium points without GOACP, the equatorial off-axis equilibrium points in Wang and Xu [24] have extended the longitude range of equilibrium points around an asteroid, while in-plane non-equatorial equilibrium points here have extended the latitude range.

However, it is easy to find that the extension of longitude range by the equatorial off-axis equilibrium points in Wang and Xu [24] is larger than the extension of latitude range by the non-equatorial equilibrium points here. This is because it is only needed to null out the second-order C_{22} term of the asteroid's gravity to extend the longitude range of equilibrium points within the equatorial plane in Wang and Xu [24], whereas it is needed to null out the zeroth-order Kepler two-body term of the asteroid's gravity to extend the latitude range of equilibrium points within the longitudinal principal plane in this paper.

5.2.3 Second family of non-equatorial equilibrium points

Although the GOACP is considered in the attitude-restricted orbital dynamics, our calculation has suggested that the existence condition of the second family of non-equatorial equilibrium points is not changed much compared with the classical condition without $\boldsymbol{\alpha}_{\mathrm{OAC}}$ given by Eqs. (35) and (39). This is because the GOACP is a higher-order term compared with the zeroth-order Kepler two-body term of the asteroid's gravity.

Therefore, in the following we will give a calculation example in the case of $\tau_0 > 2\tau_2$ and $\tau_0 < 0$, which permits existence of the second family of non-equatorial equilibrium points even when the GOACP is weak with a small ρ. However, it deserves our special attention that, according to the definition of τ_0 and τ_2 in Wang and Xu [24], $0 > \tau_0 > 2\tau_2$ means $I_{\mathrm{P},xx} > I_{\mathrm{P},zz} > I_{\mathrm{P},yy}$, i.e., the asteroid is rotating around its intermediate-moment principal axis. This case cannot exist in the solar system, since the asteroid will be tumbling under arbitrarily small perturbative torques. This point has been overlooked by Howard [26] in his study on classical non-equatorial equilibrium points. Although $0 > \tau_0 > 2\tau_2$ is not a real case in the solar system, our following study will still provide some meaningful theoretical results on the in-plane non-equatorial equilibrium points.

The parameters of the asteroid are chosen as follows:

$$\begin{aligned} &\mu = 5\ \mathrm{m}^3/\mathrm{s}^2, \quad C_{20} = -0.15, \quad C_{22} = -0.1, \\ &a_e = 250\ \mathrm{m}, \quad \omega_T = 2.9089 \times 10^{-4}\ \mathrm{s}^{-1} \end{aligned} \tag{48}$$

where the parameters are the same as in Section 5.2.1, except C_{20} and C_{22}.

As in Section 5.2.1, the mass distribution of the spacecraft is set to be $I_{xx} : I_{yy} : I_{zz} = 1.5 : 1.2 : 1$, and the five values of spacecraft's characteristic dimension ρ are chosen as 0 m, 2 m, 50 m, 100 m, and 160 m, where $\rho = 0$ m corresponds to the classical point-mass orbital dynamics without GOACP.

By using method (c), iteration method II, the second family of non-equatorial equilibrium points can be obtained through the iteration procedure with equilibrium points in Section 5.1.3 as the initial guesses. We then plot the loci of the second family of non-equatorial equilibrium points in the asteroid's $\boldsymbol{u}$–$\boldsymbol{w}$ plane with respect to the attitude angle $0 \leqslant \theta \leqslant \pi$ in the cases of different ρ. The loci are given in Figs. 7–11, respectively.

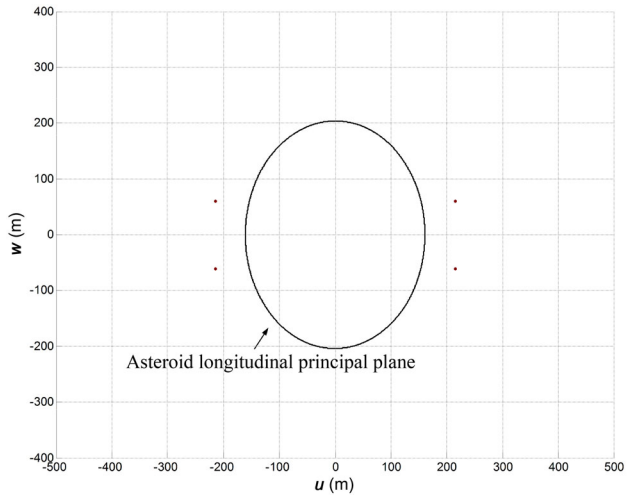

Fig. 7 Classical non-equatorial equilibrium points in point-mass orbital dynamics without GOACP.

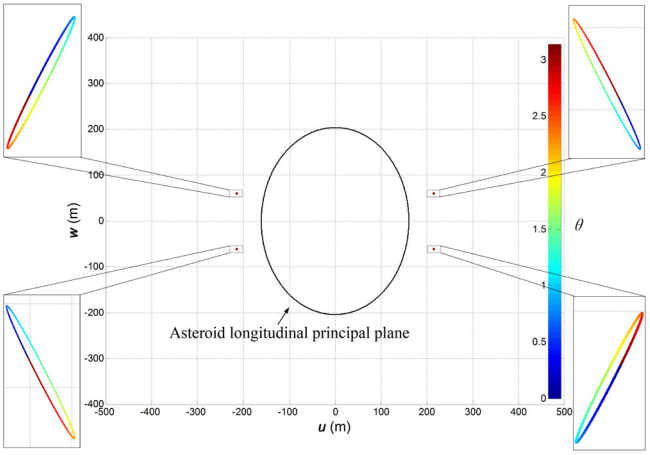

Fig. 8 Loci of the second family of non-equatorial equilibrium points in the case of $\rho = 2$ m.

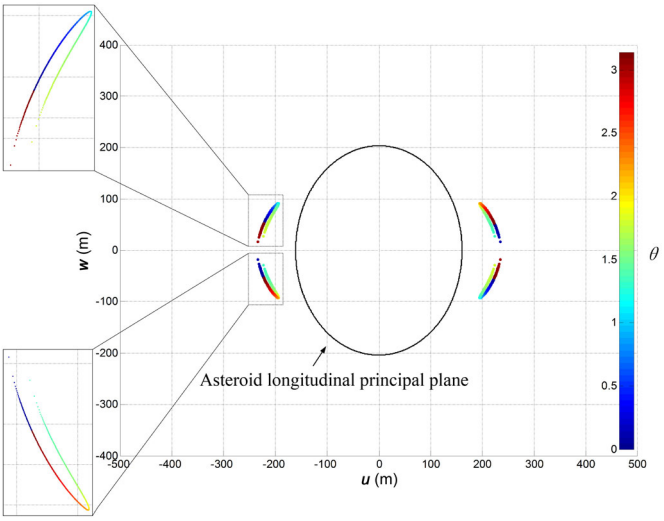

Fig. 9 Loci of the second family of non-equatorial equilibrium points in the case of $\rho = 50$ m.

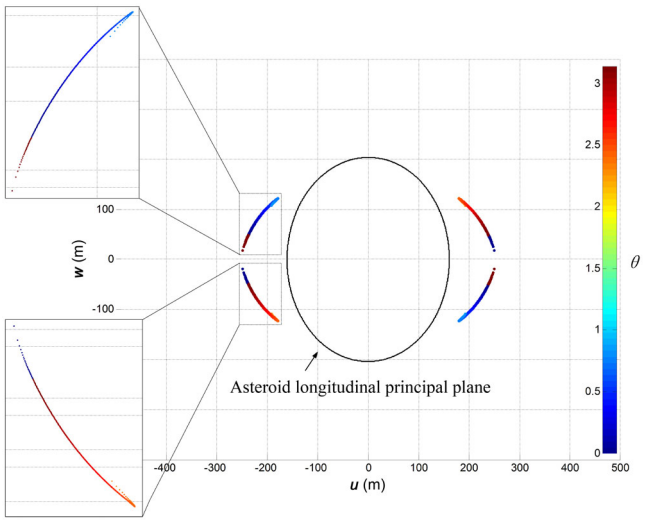

Fig. 10 Loci of the second family of non-equatorial equilibrium points in the case of $\rho = 100$ m.

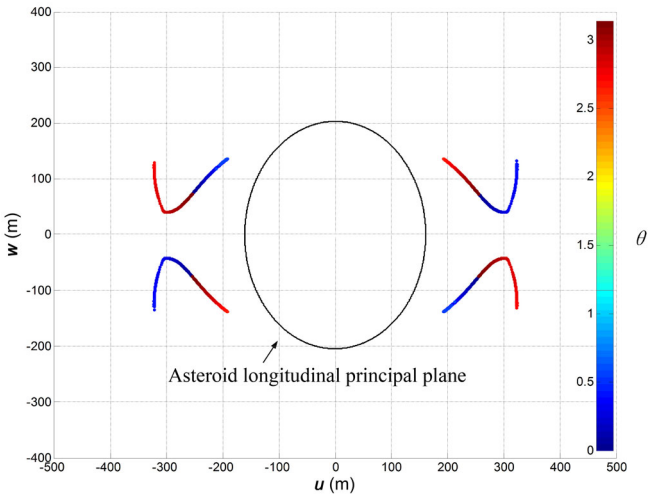

Fig. 11 Loci of the second family of non-equatorial equilibrium points in the case of $\rho = 160$ m.

5.2.4 Discussions on second family

Unlike the first family, the second family of non-equatorial equilibrium points can only exist in the $\boldsymbol{u}$–$\boldsymbol{w}$ plane of the asteroid, i.e., the principal plane spanned by $\boldsymbol{w}$-axis and the shorter equatorial principal axis.

According to Figs. 7–11, as in Section 5.2.2, some similar conclusions about the second family of non-equatorial equilibrium points can be drawn:

(a) The second family of non-equatorial equilibrium points in Figs. 8–11 is the generalization of classical ones without GOACP given by Eqs. (35) and (38), and Fig. 7. The loci of the second family are consisted of four isolated parts, which are located within four quadrants of the $\boldsymbol{u}$–$\boldsymbol{w}$ plane, respectively.

(b) The loci of the second family also have some symmetries: The loci are symmetrical with respect to the asteroid's $\boldsymbol{u}$-axis and $\boldsymbol{w}$-axis due to the symmetries of mass distributions of the asteroid and the spacecraft; for a given value of attitude angle θ, four corresponding non-equatorial equilibrium points are located on the four isolated parts of loci within four quadrants of the $\boldsymbol{u}$–$\boldsymbol{w}$ plane, respectively. The equilibrium points in the first and third quadrants are symmetrical with respect to the asteroid's center, and those in the second and fourth quadrants are also symmetrical.

(c) The GOACP $\boldsymbol{\alpha}_{\mathrm{OAC}}$ is weak in the case of $\rho = 2$ m, and then the second family is close to the classical non-equatorial equilibrium points without $\boldsymbol{\alpha}_{\mathrm{OAC}}$, as shown by Figs. 7 and 8. In Figs. 8–11, as ρ increases to 160 m, the GOACP $\boldsymbol{\alpha}_{\mathrm{OAC}}$ becomes more and more significant. Consequently, the loci of the second family expand from the vicinity of classical non-equatorial equilibrium points without $\boldsymbol{\alpha}_{\mathrm{OAC}}$, the latitude range of which is extended by the second family.

(d) As shown by Fig. 8, in the case of a small ρ, the loci of the second family are four closed curves around the classical non-equatorial equilibrium points without $\boldsymbol{\alpha}_{\mathrm{OAC}}$. As ρ increases, the closed curves become larger. As θ changes from 0 to π, the equilibrium point will move along the closed curve for one cycle.

(e) In Figs. 9–11, as ρ becomes larger than 50 m, the GOACP $\boldsymbol{\alpha}_{\mathrm{OAC}}$ is so significant that the second family cannot exist in a subinterval near $\theta = \pi/2$. Therefore, the closed curves of the loci in the case of $\rho = 2$ m have been pulled apart near $\theta = \pi/2$, and the second family can only exist in two subintervals at the beginning and end of $0 < \theta < \pi$, as shown by Figs. 9–11. As ρ increases, the sub interval near $\theta = \pi/2$ becomes larger, and then the closed curves become more apart near $\theta = \pi/2$.

5.3 Attitude stabilization

The asteroid body-fixed hovering within a larger latitude range can be achieved with active orbital control at in-plane non-equatorial equilibrium points. However, we will encounter the same issue as in Wang and Xu [24]. In the attitude-restricted orbital dynamics, the spacecraft has been assumed to be controlled ideally to a given attitude with respect to the asteroid. At in-plane non-equatorial equilibrium points, due to the constant and biased attitude with respect to the nadir direction, a constant gravity gradient torque will be acted on the spacecraft, and the induced angular momentum needs to be absorbed consistently by the onboard attitude control system, i.e., the reaction wheels. Fuel will be needed to unload the angular momentum of reaction wheels when reaction wheels reach saturation.

Therefore, as in Wang and Xu [24], it is necessary to assess the effect of gravity gradient torque to see how much fuel will be needed to unload angular momentum of the reaction wheels. The second-order gravity gradient torque acted on the spacecraft expressed in its body-fixed frame S_{B} can be given by

$$\boldsymbol{T} = \frac{3\mu}{R^5}\boldsymbol{R} \times \boldsymbol{I}\boldsymbol{R} \tag{49}$$

where $\boldsymbol{R} = \boldsymbol{A}^{\mathrm{T}}\boldsymbol{r}$ is the spacecraft's position vector with respect to the asteroid expressed in the spacecraft's body-fixed frame S_{B}. Since the relative attitude $\boldsymbol{A}$ is a single axis rotation around the $\boldsymbol{v}$-axis, see Eq. (13), $\boldsymbol{R}$ is within the spacecraft's $\boldsymbol{i}$–$\boldsymbol{k}$ plane, and the gravity gradient torque $\boldsymbol{T}$ has non-zero component only on the $\boldsymbol{j}$-axis with components on the $\boldsymbol{i}$-axis and $\boldsymbol{k}$-axis both equal to zero.

The magnitude of gravity gradient torque per unit mass (kg) of the spacecraft for the first and second families of non-equatorial equilibrium points in Figs. 3–6, 8–11 have been calculated. Their curves versus the attitude angle θ in the cases of different ρ are given in Figs. 12 and 13.

According to Figs. 12 and 13, among the two families of non-equatorial equilibrium points, the gravity

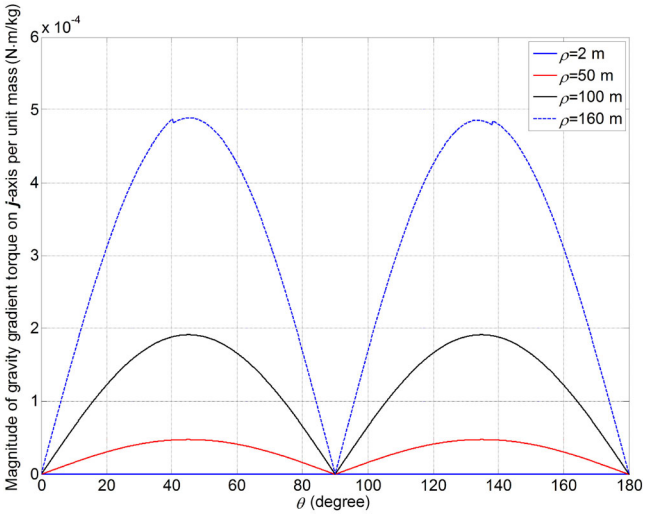

Fig. 12 Magnitude of gravity gradient torque per unit mass (kg) of spacecraft at the first family of non-equatorial equilibrium points.

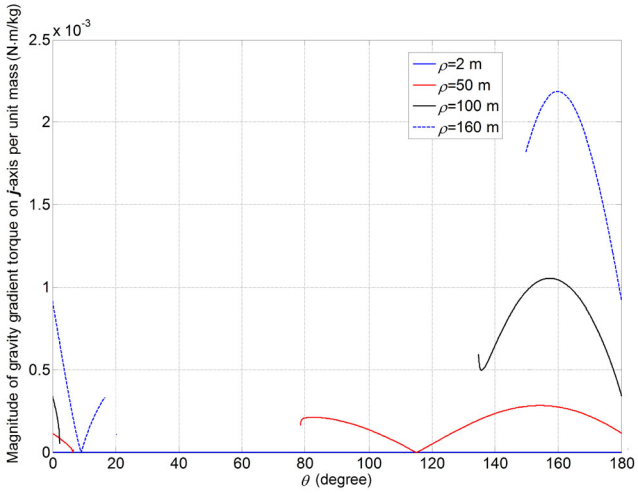

Fig. 13 Magnitude of gravity gradient torque per unit mass (kg) of spacecraft at the second family of non-equatorial equilibrium points (the part in the first quadrant).

gradient torque of the second family is larger since it is nearer to the asteroid. Notice that some curves in Fig. 13 are not complete since the second family cannot exist in a subinterval near $\theta = \pi/2$.

We can find that as the characteristic dimension ρ increases, the magnitude of gravity gradient torque increases. In the case of $\rho = 2$ m the gravity gradient torque is too small to be seen in Figs. 12 and 13. In the case of $\rho = 160$ m, the maximum magnitude of gravity gradient torque per unit mass (kg) of the spacecraft, which can be reached at the second family of equilibrium points, is about 2.2×10^{-3} N $\cdot$ m/kg. In the worst case, all the absorbed angular momentum needs to be unloaded by thrusters, and the average acceleration by thrusters to unload the angular momentum can be roughly estimated as about $2.2 \times 10^{-3}/\rho = 1.375 \times 10^{-5}$ m/s^2, which is reasonable and practical. In a better case, before the reaction wheels reach saturation, the angular momentum can be stored temporarily and be unloaded in later mission operations by the gravity gradient torque in an opposite direction. Therefore, the issue of consistently absorbed angular momentum by reaction wheels can be solved by the momentum-unloading thrusters.

5.4 Dynamical simulation

In this subsection, we will show a dynamical simulation to verify the in-plane non-equatorial equilibrium points obtained above. The parameters of the asteroid and spacecraft are chosen as Eqs. (45) and (46), and $\rho = 160$ m.

A non-equatorial equilibrium points in the $\boldsymbol{u}$–$\boldsymbol{w}$ plane of the asteroid obtained in Subsection 5.2.1 is selected. The oscillating motion about the equilibrium point can be used as the verification of the equilibrium. The chosen non-equatorial equilibrium points in the $\boldsymbol{u}$–$\boldsymbol{w}$ plane are as follows:

$$\boldsymbol{r}_e = [395.04,\ 0,\ 2.13]^{\mathrm{T}}\ \mathrm{m}, \quad \theta = 4.5^{\circ} \tag{50}$$

The initial positions of the spacecraft are chosen to be slightly away from the non-equatorial equilibrium points as follows, respectively:

$$\boldsymbol{r}_0 = [394.5,\ 0,\ 2]^{\mathrm{T}}\ \mathrm{m}, \quad \dot{\boldsymbol{r}}_{01} = [0,\ 0,\ 0]^{\mathrm{T}} \tag{51}$$

The trajectory of spacecraft is shown in Fig. 14. The non-equatorial equilibrium point is denoted by a star (*) in the figure. The oscillation of the spacecraft's position has verified the non-equatorial equilibrium point.

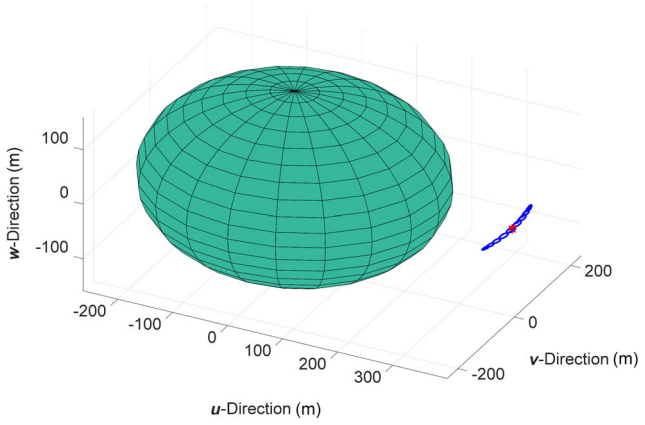

Fig. 14 Trajectory of the spacecraft about the non-equatorial equilibrium point.

6 Conclusions

In the present paper, we have investigated the in-plane non-equatorial equilibrium points of attitude-restricted orbital dynamics near asteroids, which are within the asteroid's longitudinal principal plane. The attitude-restricted orbital dynamics is a recently proposed proximity orbital dynamics model about asteroids, in which the perturbation caused by GOACP is taken into account besides the asteroid's non-spherical gravity.

The in-plane non-equatorial equilibrium points require that one of the spacecraft's principal planes is parallel to the asteroid's longitudinal principal plane. Based on the derived equilibrium condition, three methods to calculate non-equatorial equilibrium points

have been given, including solving the algebra equation system by fsolve in the software MATLAB, iteration method I, and iteration method II.

By using the three methods, we have determined two families of in-plane non-equatorial equilibrium points, and plotted their loci with respect to the attitude angle. By taking GOACP into account, the first and second families of non-equatorial equilibrium points are generalizations of, and are located around, the classical equatorial on-axis equilibrium points and non-equatorial equilibrium points in the point-mass orbital dynamics without GOACP, respectively.

The loci of non-equatorial equilibrium points have shown that compared with the point-mass orbital dynamics without GOACP, in-plane non-equatorial equilibrium points have extended the latitude range of classical equilibrium points. However, the extension of latitude range here is smaller than the extension of longitude range by equatorial off-axis equilibrium points in the previous paper. This is because only the C_{22} term of the asteroid's gravity is needed to be null out to extend the longitude range of equilibrium points within the asteroid's equatorial plane, whereas the Kepler two-body term is needed to be null out to extend the latitude range of equilibrium points within the longitudinal principal plane.

It has been shown that the GOACP makes the phase space of attitude-restricted orbital dynamics more complicated than that of the classical point-mass orbital dynamics. Equatorial equilibrium points obtained before and in-plane non-equatorial equilibrium points obtained here give a complete map of the equilibrium points in the asteroid's principal planes. More importantly, non-equatorial equilibrium points can provide natural hovering positions in a wider latitude range. In the future, it will be of great interest to study the orbital control via GOACP by the attitude control system.

Acknowledgements

Yue Wang thanks the Editor-in-Chief Professor Bong Wie and two anonymous reviewers for their constructive comments and suggestions to improve this paper signifi-cantly. This work has been supported by the National Natural Science Foundation of China under Grant Nos. 11602009, 11432001, and 11872007, the Young Elite Scientist Sponsorship Program by China Association for Science and Technology under Grant No. 2017QNRC001, and the Fundamental Research Funds for the Central Universities.

References

[1] Scheeres, D. J. Spacecraft at small NEO. *arXiv reprint*, physics/0608158, **2006**.

[2] Wang, Y., Xu, S. J. Gravitational orbit-rotation coupling of a rigid satellite around a spheroid planet. *Journal of Aerospace Engineering*, **2014**, 27(1): 140–150.

[3] Scheeres, D. J. Orbit mechanics about asteroids and comets. *Journal of Guidance, Control, and Dynamics*, **2012**, 35(3): 987–997.

[4] Scheeres, D. J. Orbital mechanics about small bodies. *Acta Astronautica*, **2012**, 72: 1–14.

[5] Scheeres, D. J. Orbital motion in strongly perturbed environments. Berlin, Heidelberg: Springer-Verlag Berlin Heidelberg, **2012**.

[6] Scheeres, D. J. Close proximity dynamics and control about asteroids. In: Proceedings of the 2014 American Control Conference, **2014**.

[7] Russell, R. Survey of spacecraft trajectory design in strongly perturbed environments. *Journal of Guidance, Control, and Dynamics*, **2012**, 35(3): 705–720.

[8] Jiang, Y., Yu, Y., Baoyin, H. X. Topological classifications and bifurcations of periodic orbits in the potential field of highly irregular-shaped celestial bodies. *Nonlinear Dynamics*, **2015**, 81(1–2): 119–140.

[9] Riverin, J. L., Misra, A. Attitude dynamics of satellites orbiting small bodies. In: Proceedings of the AIAA/AAS Astrodynamics Specialist Conference and Exhibit, **2002**: AIAA 2002-4520.

[10] Misra, A. K., Panchenko, Y. Attitude dynamics of satellites orbiting an asteroid. *The Journal of the Astronautical Sciences*, **2006**, 54(3–4): 369–381.

[11] Kumar, K. D. Attitude dynamics and control of satellites orbiting rotating asteroids. *Acta Mechanica*, **2008**, 198(1–2): 99–118.

[12] Wang, Y., Xu, S. J. Equilibrium attitude and nonlinear attitude stability of a spacecraft on a stationary orbit around an asteroid. *Advances in Space Research*, **2013**, 52(8): 1497–1510.

[13] Sincarsin, G. B., Hughes, P. C. Gravitational orbit-attitude coupling for very large spacecraft. *Celestial Mechanics*, **1983**, 31(2): 143–161.

[14] Wang, L. S., Krishnaprasad, P. S., Maddocks, J. H. Hamiltonian dynamics of a rigid body in a central gravitational field. *Celestial Mechanics & Dynamical Astronomy*, **1990**, 50(4): 349–386.

[15] Wang, L. S., Maddocks, J. H., Krishnaprasad, P. S. Steady rigid-body motions in a central gravitational field. *Journal of the Astronautical Sciences*, **1992**, 40(4): 449–478.

[16] Sanyal, A. K. Dynamics and control of multibody systems in central gravity. Ph.D. Dissertation. Ann Arbor, MI: Department of Aerospace Engineering, the University of Michigan, **2004**

[17] Teixidó Román, M. Hamiltonian methods in stability and bifurcations problems for artificial satellite dynamics. Master Thesis Barcelona: Facultat de Matemàtiques i Estadística, Universitat Politècnica de Catalunya, **2010**: 51–72.

[18] Wang, Y., Xu, S. J. Symmetry, reduction and relative equilibria of a rigid body in the J2 problem. *Advances in Space Research*, **2013**, 51(7): 1096–1109.

[19] Wang, Y., Xu, S. J., Zhu, M. P. Stability of relative equilibria of the full spacecraft dynamics around an asteroid with orbit–attitude coupling. *Advances in Space Research*, **2014**, 53(7): 1092–1107.

[20] Lee, D., Sanyal, A. K., Butcher, E. A., Scheeres, D. J. Almost global asymptotic tracking control for spacecraft body-fixed hovering over an asteroid. *Aerospace Science and Technology*, **2014**, 38: 105–115.

[21] Lee, D., Sanyal, A., Butcher, E., Scheeres, D. Finite-time control for spacecraft body-fixed hovering over an asteroid. *IEEE Transactions on Aerospace and Electronic Systems*, **2015**, 51(1): 506–520.

[22] Misra, G., Izadi, M., Sanyal, A., Scheeres, D. Coupled orbit–attitude dynamics and relative state estimation of spacecraft near small Solar System bodies. *Advances in Space Research*, **2016**, 57(8): 1747–1761.

[23] Wang, Y., Zhong, R., Xu, S. J. Orbital perturbation due to orbit-attitude coupling near asteroids. *Aircraft Engineering and Aerospace Technology*, **2018**, 90(1): 104–113.

[24] Wang, Y., Xu, S. J. Orbital dynamics and equilibrium points around an asteroid with gravitational orbit–attitude coupling perturbation. *Celestial Mechanics and Dynamical Astronomy*, **2016**, 125(3): 265–285.

[25] Hu, W. Orbital motion in uniformly rotating second degree and order gravity fields. Ph.D. Dissertation. Ann Arbor, MI: Department of Aerospace Engineering, the University of Michigan, **2002**.

[26] Howard, J. E. Spectral stability of relative equilibria. *Celestial Mechanics & Dynamical Astronomy*, **1990**, 48(3): 267–288.

Yue Wang received his B.Eng. and Ph.D. degrees in aerospace engineering from Beihang University (formerly known as Beijing University of Aeronautics and Astronautics), Beijing, China, in 2009 and 2014, respectively. From 2014 to 2015, he worked as a postdoctoral fellow in the Distributed Space Systems Lab in the Faculty of Aerospace Engineering at Technion—Israel Institute of Technology, Haifa, Israel. In 2016, he joined the School of Astronautics at Beihang University as an associate professor of the "Zhuoyue" Recruitment Program. His research interests center on the astrodynamics, orbital dynamics, dynamics and control about asteroids, spacecraft proximity operations, and space debris mitigation. E-mail: ywang@buaa.edu.cn.

Shijie Xu (1951–2019) was not only a great researcher but also, more importantly, a great mentor and advisor in the field of astrodynamics and spacecraft control. He received his B.Eng. degree from the Department of Mechanical Engineering, Northeast Forestry University, Harbin, China, in 1976. His career in astrodynamics and spacecraft control started soon after he received his M.S. degree from the Laboratory of Flight Dynamics, Harbin Institute of Technology, Harbin, in 1983, as a teaching assistant at the same laboratory. He worked at Harbin Institute of Technology as a lecturer (1987), an associate professor (1989), and then as a professor (1993). During his tenure at Harbin Institute of Technology, he pursued his Ph.D. degree with a specialization in automatic controls from 1991 to 1995 at Henri Poincaré University, Nancy, France. From 1995 to 2000, he was with Harbin Institute of Technology as a professor. In 2000, he joined the School of Astronautics, Beihang University, Beijing, China, as a professor. He carried out research spread out in the field of astrodynamics and spacecraft control, including the robust control theory and applications, the attitude control of flexible spacecraft, attitude control via momentum exchange devices, integrated attitude control and energy management, guidance and control of proximity operations, three-body problem, spacecraft dynamics about small bodies, and etc. He authored or coauthored over 300 papers in journals and conferences. He supervised more than 70 graduate students at Harbin Institute of Technology and Beihang University who are now active in China's space industry and academia.